Electrically Conductive Silicone-Based Nanocomposites Incorporated with Carbon Nanotubes and Silver Nanowires for Stretchable Electrodes

Tae Gon Kim, Hyeon Sik Eom, Jong Hwi Kim, Jik Kyo Jung, Keon-Soo Jang,* and Seong Jae Lee*

Read Online

ACCESS | Metrics & More | Article Recommendations | Supporting Information

ABSTRACT: Stretchable electrode materials have attracted great attention as next-generation electronic materials because of their ability to maintain intrinsic properties with rare damage when undergoing repetitive deformations, such as folding, twisting, and stretching. In this study, an electrically conductive PDMS nanocomposite was manufactured by combining the hybrid nanofillers of carbon nanotubes (CNTs) and silver nanowires (AgNWs). The amphiphilic isopropyl alcohol molecules temporarily adhered simultaneously to the hydrophobic CNT and hydrophilic AgNW surfaces, thereby improving the dispersity. As the CNT/AgNW ratio (wt %/wt %) decreased under the constant nanofiller content, the tensile modulus decreased and the elongation at break increased owing to the poor interaction between the AgNWs and matrix. The shear storage moduli of all nanocomposites were higher than the loss moduli, indicating the elastic behavior with a cross-linked network. The electrical conductivities of the nanocomposite containing the hybrid nanofillers were superior to those of the nanocomposite containing either CNT or AgNW at the same filler content (4 wt %). The hybrid nanofillers were rearranged and deformed by 5000 cyclic strain tests, relaxing the PDMS matrix chain and weakening the interfacial bonding. However, the elastic behavior was maintained. The dynamic electrical conductivities gradually increased under the cyclic strain tests due to the rearrangement and tunneling effect of the nanofillers. The highest dynamic electrical conductivity (10 S/m) was obtained for the nanocomposite consisting of 2 wt % of CNTs and 2 wt % of AgNWs.
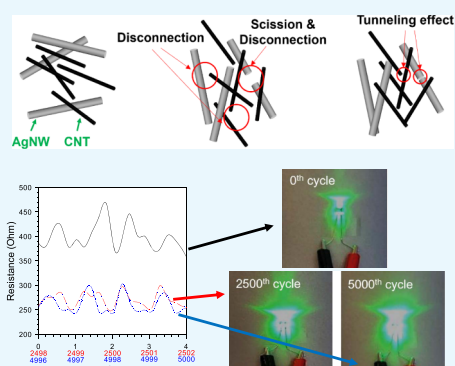
1. INTRODUCTION

Polymer nanocomposites are typically composed of a polymer matrix and nanofillers (carbon-based materials, metals, and ceramics).[1−4] When the nanofillers are homogeneously dispersed in the polymer matrix, the nanocomposite exhibits enhanced properties, such as electrical, mechanical, and thermal properties, and overcomes the property limitation of a singular material.[1,4,5] The use of nanofillers reduces the concentration of fillers to achieve the desired properties, compared to that of microfillers.[1,4] Among diverse nanocomposites, stretchable electrode materials that maintain electrical conduction via various deformations have found a use in applications, such as biodevices, sensors, batteries, and displays.[6,7] These stretchable electrode materials consist of an elastic polymer matrix and electrically conductive nanofillers.[7] The incorporation of electrically conductive nanofillers into an electrically insulating polymer matrix generates an electrical network, thereby leading to electrical conduction.[3] However, the dispersion of nanofillers in a polymer matrix is commonly poor owing to the incompatibility between the polymer/nanofillers and aggregation caused by vdW interactions between the nanofillers.[8,9] Poor dispersion brings about a reduction in various properties.[10] Thus, the interfacial interactions between the polymer and nanofillers are important

for uniform dispersion.[11] The interfacial interactions are largely dependent on the surface area, surface characteristics, and wetting parameters.[12]

Carbon nanotubes (CNTs) feature 1−5 TPa of Young's modulus, excellent thermal stability (∼2800 °C), and superior thermal (twice that of diamond), and electrical conductivities (1000 times that of copper).[13−16] CNTs are typically classified as single-walled CNTs (SWCNTs), multiwalled CNTs (MWCNTs), thin-walled CNTs (TWCNTs), and branched CNTs.[17,18] SWCNTs show superior mechanical, electrical, and thermal properties compared to MWCNTs and TWCNTs.[17] However, TWCNTs are cheaper and purer than SWCNTs and have larger aspect ratios and specific volumes than MWCNTs. Recently, the branched CNT, which is also known as the carbon nanostructure, has been introduced to piezoresistive polymer nanocomposites owing to its superior electrical conductivity.[15,18−20] Similar to other nanofillers, the dispersion

31876

of CNTs in a polymer matrix is poor because of the vdW forces between the CNTs.[21,22] Mechanical dispersion and CNT surface functionalization are chiefly utilized to homogeneously disperse the CNTs.[22,23] For mechanical dispersion, ultrasound treatment and ball milling effectively reduce the aggregation, thereby resulting in good dispersion.[24−26] However, the ball milling method impairs the CNT, although it gives a narrow length and diameter distribution.[27] For CNT surface functionalization, noncovalent and covalent functionalization methods can be used.[22,28] Surfactants and polymer chains cover the CNT surfaces, maintaining the structure and characteristics of CNTs by the noncovalent functionalization method.[29,30] For the covalent functionalization method, as an example, a carboxylic group (−COOH) is chemically attached to CNT surfaces, and thus, the dispersion is enhanced via an additional solvent or compatibilization with a polymer matrix.[31,32]

Silver nanowires (AgNWs) feature an aspect ratio of >10 with 1D, excellent electrical, optical, and thermal properties.[33] AgNWs can be used for photovoltaic cells, displays, and flexible electrodes.[34−36] AgNWs can be synthesized using nanoporous membranes, electron-beam spinning, and the polyol method.[36,37] Among the AgNW production methods, the polyol method is the most facile for large−quantity production.

The stretchability of conductive polymer nanocomposites is largely determined by the elastomeric matrix. Suitable matrix materials include PDMS, thermoplastic polyurethane, and hydrogels. Among them, PDMS is the most widely used matrix for stretchable nanocomposites.[38,39] On the other hand, the electrical conductivity of the stretchable nanocomposite is determined by the conductive nanofiller. Suitable nanofiller materials include carbon-based nanomaterials such as CNTs, graphene,[40] and metallic nanomaterials, such as AgNWs, gold nanowires, and copper nanowires.[39,41] In addition to single-component conductive nanofillers, hybrid nanofillers have been used to enhance the electrical and mechanical properties of stretchable conductive polymer nanocomposites through synergistic effects between heterogeneous nanofillers.[42−45] The combination of AgNWs and graphene as hybrid fillers in polymer matrices generated piezoresistive polymer nanocomposites for potential applications such as wearable devices, electronic skins, motion (strain) sensors, and healthcare and human-machine interfacing applications.[45−51] However, most of the hybrid nanofillers studied so far consisted of AgNW and graphene combinations. In this study, AgNWs were synthesized via the polyol method, and the AgNWs and TWCNTs were simultaneously compounded with PDMS to generate stretchable electrode nanocomposites with high electrical conductivity. The dispersion of the conductive nanofillers was enhanced by multidispersion steps. We examined the correlation between the dispersion and properties, such as mechanical, rheological, and electrical properties under cyclic deformation.

2. EXPERIMENTAL SECTION

2.1. Materials. CNTs (TWCNTs, Jenotube 6A) were purchased from JEIO Co. (South Korea). Silver nitrate (AgNO_3, 99.9%) was obtained from Kojima Chemicals Co. (Japan). PVP (MW: 1,300,000 g/mol) and tetrapropylammonium chloride (TPAC, 98%) were purchased from Sigma-Aldrich (St. Louis, MO, USA). Ethylene glycol (EG, 99.5%) as a reductant and acetone as an aggregating agent for AgNWs

were obtained from Samchun Chemical Co. (South Korea). For PDMS matrix production, a binder (Sylgard 184A), a hardener (Sylgard 184B), and a Pt-based catalyst (included in PDMS base) were purchased from Dow Corning Co. (Midland, MI, USA). Figure 1 shows the curing mechanism
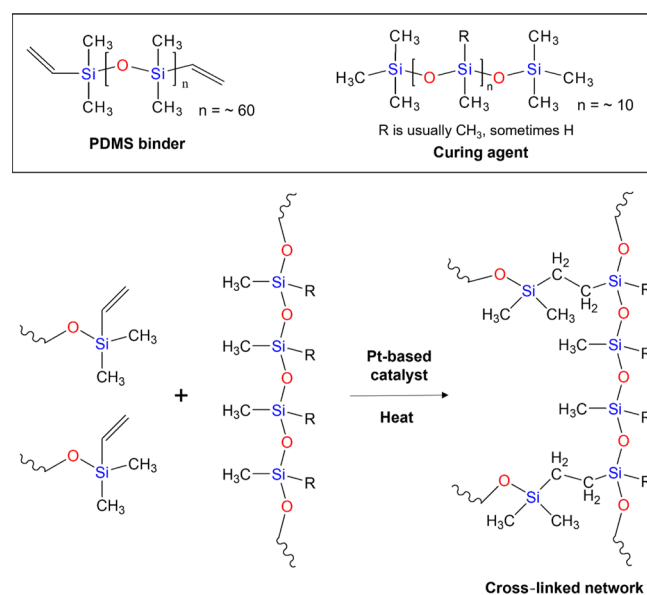
Figure 1. Chemical structure and curing mechanism of silicone thermoset resins.

of PDMS.[52] Isopropyl alcohol (IPA, 99.5%), to enhance the dispersion of CNTs and AgNWs, was purchased from Samchun Chemical Co. (South Korea). Methyl-terminated silicone oil (XIAMETER PMX-200 Silicone Fluid, 100 cSt) was purchased from Dow Corning Co. (Midland, MI, USA). DI water was purified by Option-Q (Purelab, ELGA, High Wycombe, UK).

2.2. Synthesis and Purification of AgNWs. *2.2.1. Synthesis of AgNWs.* AgNWs were synthesized via the polyol reduction method. A solution of 0.045 M PVP in 92 mL of EG was prepared and stirred at 120 rpm for 30 min. Subsequently, 0.025 M AgNO_3 in EG was added to the solution and stirred at 120 rpm for 30 min. Afterward, 0.006 M TPAC in EG was added dropwise at 0.24 mL/min for 20 min. The final mixture was stirred at 180 °C for 90 min. The reaction was completed by quenching the reagents and purified by the following methods. Table 1 presents the formulation for the synthesis of AgNWs.

Table 1. Formulation for the Synthesis of AgNWs

materials	content
EG	92 mL
PVP	0.045 M
AgNO_3	0.025 M
EG/TPAC	4.8 mL (0.006 M)

2.2.2. Purification of AgNWs. Ag particles, Ag nanorods, unreacted reagents, and other impurities remained after the reaction. The solution was mixed with acetone at a ratio of 1:9 (solution/acetone) and purified by centrifugation to remove EG (reductant). The precipitated PVP-capped AgNW aggregates were redispersed in DI water. Excess acetone was

added to the solution, thereby bringing about further aggregation due to the vdW forces between the AgNWs. The Ag particles and Ag nanorods were suspended in the upper position of acetone. The Ag particles and Ag nanorods were then removed, and the precipitated AgNW aggregates were redispersed in DI water. This process was repeated five to seven times. The purified AgNWs were cleaned three times via centrifugation at 2500 rpm for 10 min, and afterward, the AgNWs dispersed in IPA were stored in DI water. The purification process is shown in Figure S1.

2.3. Fabrication of PDMS/CNT/AgNW Nanocomposites. *2.3.1. Dispersion of CNTs and AgNWs.* PDMS was partially dissolved in IPA, and CNTs/AgNWs were dispersed in IPA. CNTs/AgNWs and IPA were mixed at a ratio of 1:100 (wt/wt) and stirred at 700 rpm for 1 h. Subsequently, the mixture was ultrasonicated (25 W) for homogeneous dispersion for 150 min. 10 g of silicone oil was added to the mixture and ultrasonicated (25 W). 40 g of PDMS was added to the mixture and ultrasonicated for 90 min. The formulation and procedure for nanocomposite fabrication are shown in Table 2 and Figure 2, respectively.

Table 2. Formulation for the Preparation of the PDMS/CNT and AgNW Nanocomposite

materials	content
CNT and AgNW	2.25 g (4 wt %)
silicone oil	10 g (18 wt %)
PDMS	40 g (71 wt %)
curing agent	4 g (7 wt %)

2.3.2. Solvent Removal and Curing of the PDMS/CNT/AgNW Nanocomposites. Next, 80% of the IPA in the mixture (PDMS/CNT/AgNW in IPA) was removed by a rotary evaporator (Rotavapor R-100, BUCHI, Flawil, Switzerland) at 70 °C. The ratio between the PDMS and curing agent was 10:1. The mixture containing the PDMS and curing agent was mixed for 10 min. Subsequently, the residual IPA in the resulting mixture was removed in a vacuum oven at 45 °C. The final PDMS/CNT/AgNW precursor mixture without IPA was compressed/cured at 100 °C for 1 h to fabricate the PDMS/CNT/AgNW nanocomposite sheet with dimensions of 180 × 180 × 1 mm.

2.4. Characterization. *2.4.1. Morphological Analysis.* The morphological analysis of CNTs, AgNWs, and nanocomposites was performed by using FESEM (Apreo, FEI, Hillsboro, OR, USA). The specimens of the PDMS/CNT/AgNW nanocomposites for cross-sectional SEM studies were cryofractured to minimize the morphological deformation of the matrix during fracture. The electron beam voltage was set at 5 kV. The specimens were sputter-coated with platinum prior to the SEM analysis.

2.4.2. Dispersion Analysis. The dispersion of CNTs (0.1 wt %) in IPA was analyzed based on the measured transmittance using a UV−vis spectrometer (LAMBDA 750, PerkinElmer, Waltham, MA, USA). The dispersibility of CNTs was monitored as a function of time. The effect of the silicone oil was investigated on the basis of CNTs (0.01 wt %) in IPA using the UV−vis spectrometer. The dispersibility of nanofillers in the PDMS matrix was examined by FESEM. The dispersion of AgNWs in the PDMS matrix was further investigated by EDS dot mapping equipped with FESEM. The images were obtained at a beam current of 10 μA, scan number of four, dwell time of 1000 μs, voltage of 10 kV, and magnification of ×5,000.

2.4.3. Mechanical Properties. Tensile properties, such as tensile strength, modulus, and elongation at break of the pristine PDMS and PDMS/CNT/AgNW nanocomposites, were measured using a universal testing machine (UTM; LR10K PLUS, LLOYD Instruments, West Sussex, UK) according to ASTM D412. The specimens with dimensions of 115 mm (gauge length: 33 mm) × 25 mm × 6 mm were tested at a speed of 500 mm/min at 22−24 °C.

2.4.4. Rheological Properties. A rotational rheometer equipped with parallel plate geometry (MCR 300, Anton Paar, Graz, Austria) was used in its small-amplitude oscillatory shear mode at 25 °C and a strain amplitude of 0.1%. The frequency was varied from 0.01/s to 100/s to investigate the rheological properties of nanocomposites.

2.4.5. Electrical Properties. The electrical resistances of the PDMS/CNT/AgNW nanocomposites were measured using a picoammeter (Keithley 6487, Keithley Instruments, Solon,
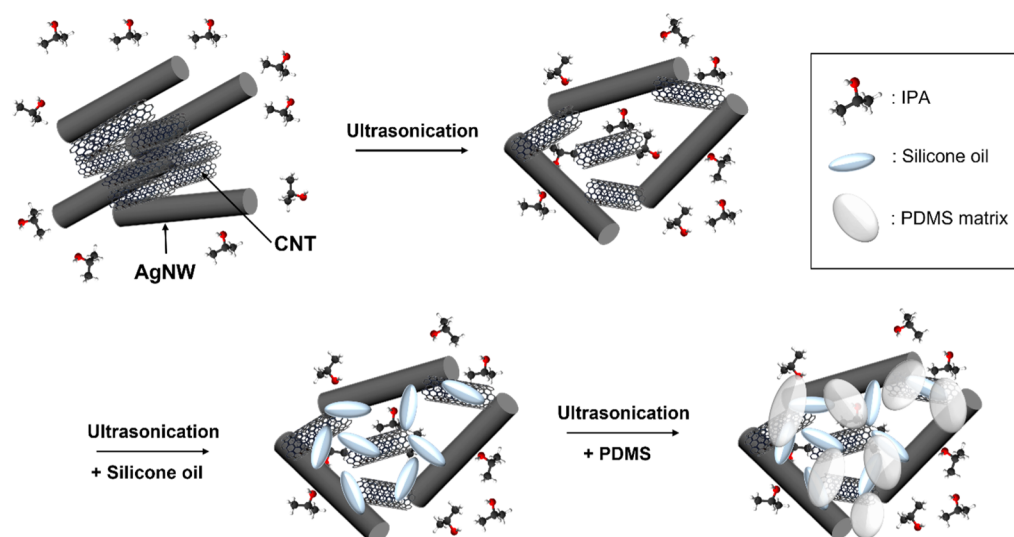
Figure 2. Schematic diagram illustrating the fabrication of the PDMS/CNT/AgNW nanocomposite.

OH, USA) and a digital multimeter (Fluke 189, Fluke, Everett, WA, USA) for sample resistances of >500 and <500 MΩ, respectively. The sheet resistances were measured using a four-point probe (M4P-302, MS Tech, South Korea) with a source measurement unit (Keithley 2400, Keithley, Solon, OH, USA). Both sides of the specimens with dimensions of 10 × 10 × 1 mm were polished with sandpaper to eliminate polymer-rich skin layers. Subsequently, a silver paste (Elcoat P-100, CANS, Japan) was coated on both sides prior to the resistance measurements. The electrical conductivities of the nanocomposites were determined based on the following equation

$$\sigma = \frac{1}{\rho} = \frac{d}{RS} \tag{1}$$

where σ, ρ, R, S, and d are the electrical conductivity, resistivity, resistance, cross-sectional area, and thickness of the sample, respectively.

2.4.6. Cyclic Deformation Properties. Dynamic properties during the cyclic deformation of the neat PDMS and PDMS/CNT/AgNW nanocomposites were investigated using a fatigue testing machine (Electro Force 5500, TA Instruments, New Castle, DE, USA). Specimens with dimensions of 66 mm (gauge length: 30 mm) × 10 × 1 mm were fabricated. The specimens were tested under 40% deformation. The dynamic properties of the samples were obtained during a cyclic strain test of 5000 cycles. The dynamic electrical resistances were measured using a picoammeter (Keithley DMM6500, Keithley Instruments, Solon, OH, USA). The electrical conductivities of the nanocomposites during cyclic strain tests were calculated using eq 1.

3. RESULTS AND DISCUSSION

3.1. Morphology of CNTs and AgNWs. The morphologies of the CNTs and synthesized AgNWs were investigated by FESEM. A uniform diameter and high aspect ratio of CNTs were observed, as shown in Figure 3. The 1D AgNWs were synthesized by the polyol method. The architecture and aspect ratio of AgNWs can be affected by various factors, such as reagent concentration, reaction temperature, and time. The
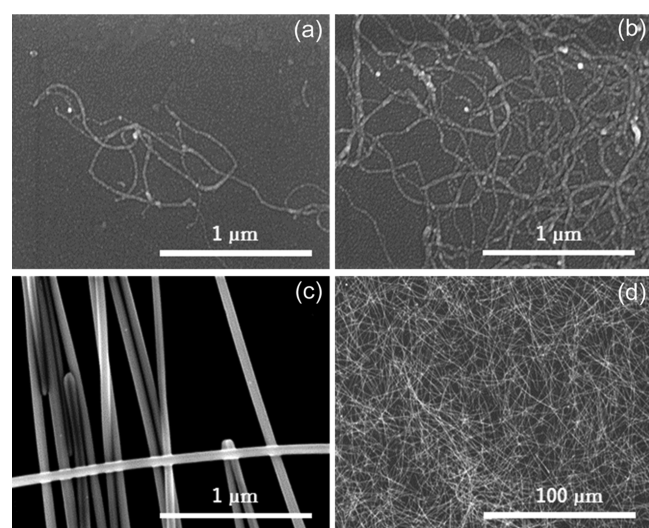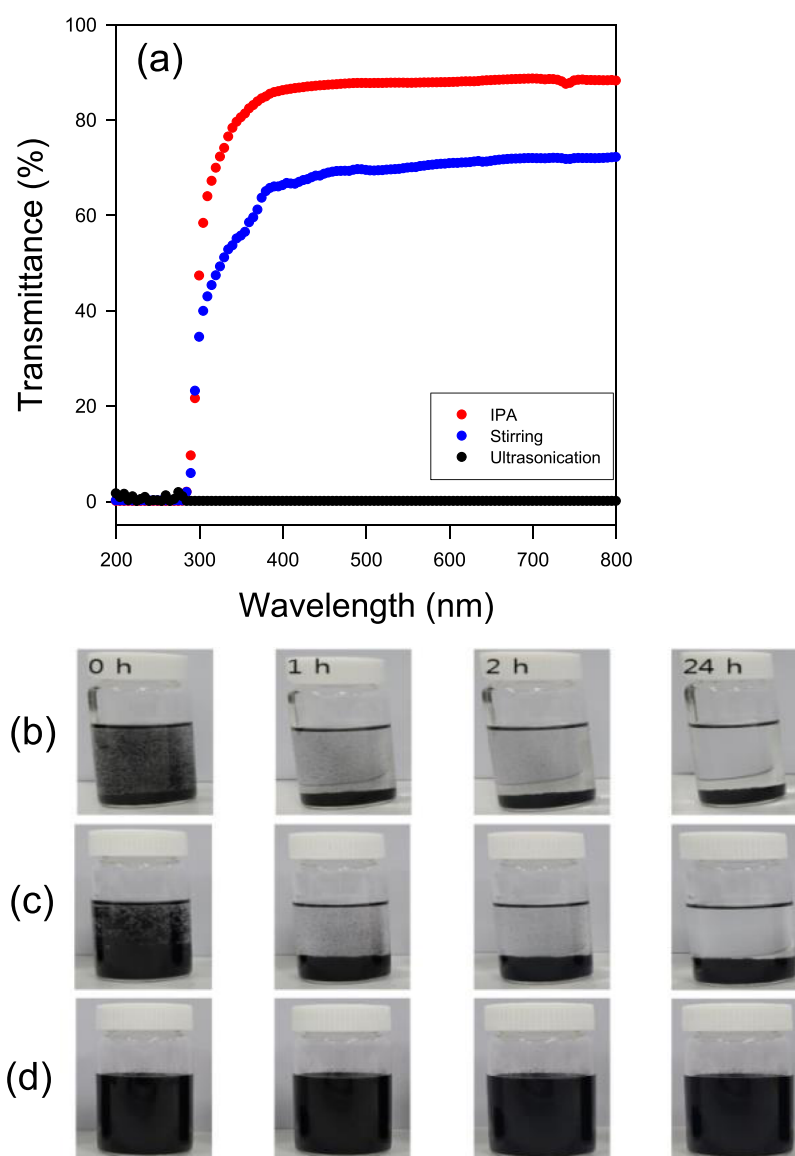
synthesized AgNWs had a mean diameter of 62 ± 6.5 nm and a length of 37 ± 8.8 μm. The aspect ratio was ca. 600.

3.2. Dispersion of CNTs and AgNWs. *3.2.1. Ultrasonication Effect on Dispersion of AgNWs and CNTs in IPA by Ultrasonication.* The dispersion of CNTs and AgNWs in a solvent was routinely investigated by SEM and TEM. Although these methods provide visual observation, quantification by SEM and TEM for dispersibility is limited. Therefore, in this study, the dispersion of CNTs in a solvent was quantified using UV−vis spectroscopy by detecting the absorption and scattering of light. IPA was chosen as a solvent owing to its amphiphilic characteristic. The dispersion of CNTs in IPA was more homogeneous than that in water and EG, as shown in Figure S2. When the CNTs are more homogeneously dispersed in IPA, the effective surface area of CNTs increases, thereby decreasing the transmittance.[53,54] The PVP-capped AgNWs were homogeneously dispersed in IPA without any treatment due to the hydrophilicity of PVP, as shown in Figure S3. In general, CNTs are heterogeneously dispersed, and thus, treatments are required to enhance the CNT dispersity. All images regarding CNT dispersion in IPA were obtained immediately after stirring. The transmittance of CNTs in IPA with stirring increased from 0 to 66% in the range of 280−380 nm and approached a steady value at a wavelength of 380 nm (Figure 4a). The transmittances of the other samples treated at a wavelength of 380 nm are listed and compared, as shown in Figure 4a. The transmittance of the pure IPA was 85%. The transmittances of the samples (CNTs in IPA) with stirring at 700 rpm for 1 h and additional ultrasonication treatment for 150 min were 66 and 0.1%, respectively. The combination of stirring and ultrasound treatments afforded the most homogenous dispersion of CNTs in IPA. The dispersion stability is shown in Figure 4b−d. The CNT/IPA mixtures without treatment and with stirring treatment showed aggregation and precipitation at 0 h, and the precipitation continued as a function of time. In contrast, the CNT/IPA mixture with the combination of stirring and ultrasonication treatments showed good dispersion stability as a function of time up to 24 h. The combination of stirring and ultrasonication treatments reduced the vdW forces between the CNTs, thereby causing the interaction between the amphiphilic IPA and CNT surfaces. Additional ultrasonication treatment effectively dispersed and stabilized CNTs in IPA without using a dispersant.[55]

3.2.2. Effects of the Silicone Oil on CNT Dispersion in PDMS. In this study, methyl-terminated silicone oil was utilized as a dispersant to further disperse the CNTs in the cured PDMS matrix. Figure 5 shows the transmittance of the neat cured PDMS, PDMS/silicone oil, PDMS/CNT, and PDMS/CNT/silicone oil. The cured PDMS and PDMS/silicone oil showed identical transmittance over the entire wavelength range (300−800 nm) measured by UV−vis spectroscopy, which indicates that the silicone oil barely influenced the transmittance of PDMS. In contrast, the effect of the silicone oil in the CNT-embedded PDMS on the transmittance was observed. The transmittance of the PDMS/CNT/silicone oil composite was lower than that of the PDMS/CNT without the silicone oil over the entire wavelength range, indicating a more homogeneous dispersion of CNTs in the cured PDMS matrix owing to the dispersant, silicone oil. This result is because the methyl-terminated silicone oil was covered on the CNT surfaces, and the core−shell CNT−silicone oil was well

Figure 3. FESEM images of CNTs (a,b) and AgNWs synthesized by the polyol process at magnifications of ×100,000 (c) and ×1000 (d).

Figure 4. Transmittance of pure IPA and IPA/CNT with stirring and ultrasonication (a) and dispersion stability of IPA/CNT for different treatment conditions: (b) no treatment, (c) stirring, and (d) stirring/ultrasonication.
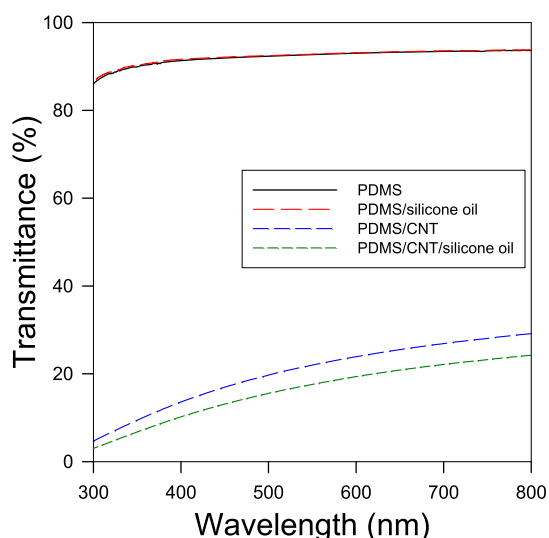
dispersed in the PDMS matrix, showing the coupling effect of the silicone oil between the PDMS matrix and CNT.[21,55]

3.2.3. Morphology of PDMS/CNT/AgNW Nanocomposites. The dispersion of nanofillers, such as CNTs and AgNWs in the cured PDMS matrix was investigated by FESEM. The filler concentration (4 wt %) used in this study was determined on the basis of the balance between mechanical and electrical properties, as shown in Table S1 and Figure S4. The dispersion of AgNWs was additionally examined by EDS mapping equipped with FESEM. The nanofillers were relatively homogeneously dispersed in the PDMS matrix, as shown in Figure 6, whereas the PDMS/AgNW nanocomposite without CNTs exhibited low dispersion with AgNW aggregates in the cured PDMS matrix. The PVP-capped AgNWs exhibited hydrophilic surfaces attributed to the PVP, and thus, they exhibited weak physical interactions with the hydrophobic PDMS matrix.[56] However, the combination of CNTs and AgNWs resulted in strong interactions among CNTs, AgNWs, and PDMS because the hydrophobic and hydrophilic parts of IPA interacted with CNTs and AgNWs, respectively, during

the dispersion process. Therefore, as the CNTs were homogeneously dispersed in the PDMS matrix, the AgNWs were also well dispersed in the matrix simultaneously. The incorporation of CNTs into the PDMS/AgNW nanocomposite afforded better dispersibility of the nanofillers in the PDMS matrix.[11]

3.3. Mechanical Properties of PDMS/CNT/AgNW Nanocomposites. The mechanical properties of nanocomposites were typically examined using a UTM. The tensile strength, tensile modulus, and elongation at break of the cured PDMS/CNT/AgNW nanocomposites were measured as a function of the CNT/AgNW ratio, as shown in Figures 7 and S5 and Table S2. P, SP, C, and A denote PDMS, silicone oil-embedded PDMS, CNT, and AgNW, respectively. For instance, SP/C1/A3 indicates the nanocomposite consisting of SP of 96 wt %, CNT of 1 wt %, and AgNW of 3 wt %.

The incorporation of silicone oil into the PDMS matrix reduced the mechanical properties owing to the plasticization effect of the silicone oil in the PDMS. The incorporation of CNTs into the silicone oil-embedded PDMS matrix increased

Figure 5. Transmittance of the PDMS matrix and PDMS/CNT nanocomposites without and with silicone oil.

the tensile strength and modulus but decreased the elongation at break. The CNTs dispersed in the matrix acted as a reinforcing agent (increase in strength and modulus) but a stress concentration source (decrease in elongation at break).[57,58] As the CNT/AgNW ratio decreased (the AgNW concentration increased), the tensile modulus decreased and the elongation at break increased. There was no significant change in tensile strength, probably because the reinforcing effects of CNTs and AgNWs were analogous.

3.4. Rheological Properties of Cured PDMS/CNT/ AgNW Nanocomposites. The CNT- or AgNW-embedded polymer nanocomposites are routinely subjected to rheological analysis to investigate their dispersibility, viscoelasticity, and microstructural transition. The rheological properties of nanocomposites are highly relevant for various applications from paints to electronics. The rheological properties are correlated with various factors, such as viscoelasticity, mixing behavior, productivity rate, energy consumption, and particle dispersion. Figure 8 shows the storage modulus (G'), complex viscosity ($\eta*$), and tan δ of the cured PDMS with and without the silicone oil and silicone oil-incorporated PDMS/CNT/ AgNW nanocomposites with different filler ratios at frequencies of 0.01−100/s. The storage moduli of all nanocomposites slightly increased as a function of frequency, which is a typical behavior of cured elastomer systems.[59] The incorporation of silicone oil into the PDMS matrix reduced the storage modulus owing to the plasticization effect of the silicone oil in the PDMS matrix, which is in good agreement with the results of the mechanical properties. The infiltration of CNTs into the PDMS/AgNW nanocomposite led to various interactions among the polymer and fillers (CNTs and AgNWs), thereby producing a complex network system. The combination of well-dispersed CNT−CNT networks and 3D networks caused by the physical/chemical interactions between CNTs and PDMS increased the storage moduli because of the dual network without morphological changes within the matrix.[5,60,61] Thus, the storage moduli of nanocomposites decreased with the decreasing CNT/AgNW ratio because the content of CNTs that enhances the dispersion of nanofillers in the PDMS matrix decreased, thereby decreasing the interactions between the nanofillers and polymer matrix.
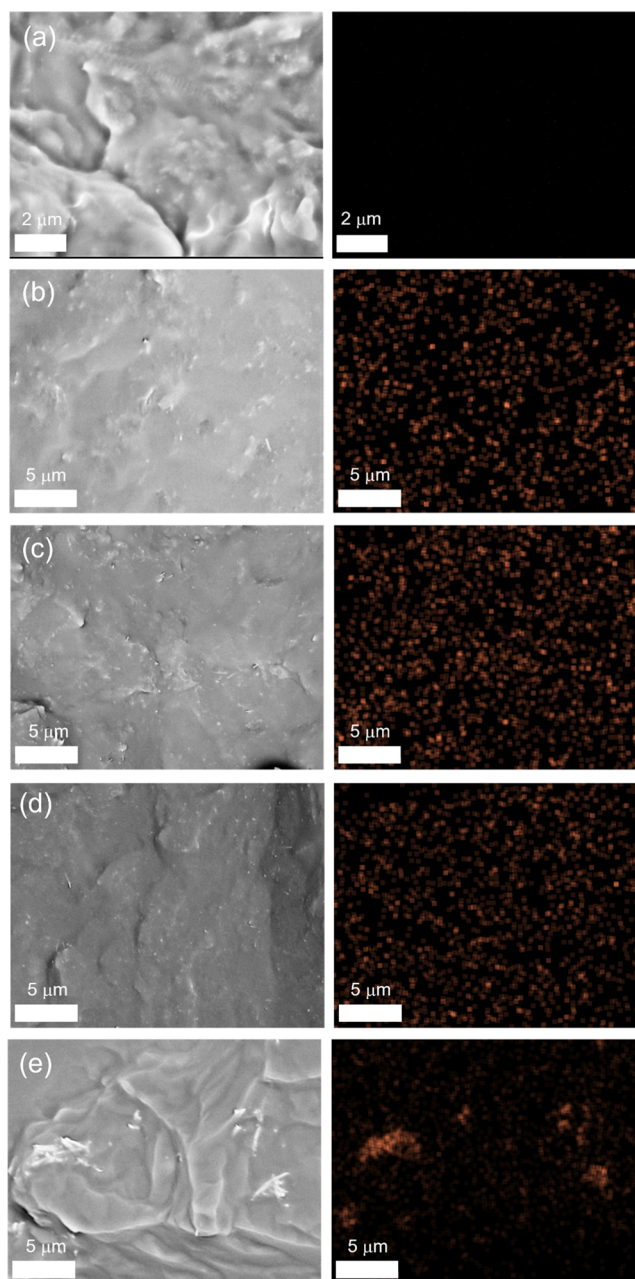

Figure 6. SEM and EDS elemental (Ag) mapping images of the fractured surfaces of the PDMS/CNT/AgNW nanocomposites with different CNT/AgNW contents (wt %/wt %): (a) C4/A0, (b) C3/ A1, (c) C2/A2, (d) C1/A3, and (e) C0/A4. C and A denote CNT and AgNW, respectively.

The AgNW-embedded PDMS nanocomposite, excluding CNTs, exhibited the AgNW aggregates and the storage modulus and complex viscosity similar to SP (silicone oil-embedded PDMS); this was because the interaction between the PDMS chains became dominant over that between the fillers and PDMS. The $\eta*$ value was calculated based on eq 2.

$$|\eta*| = \sqrt{\left(\frac{G'}{\omega}\right)^2 + \left(\frac{G''}{\omega}\right)^2} \tag{2}$$

where ω, G', and G'' are the angular frequency, storage modulus, and loss modulus, respectively.
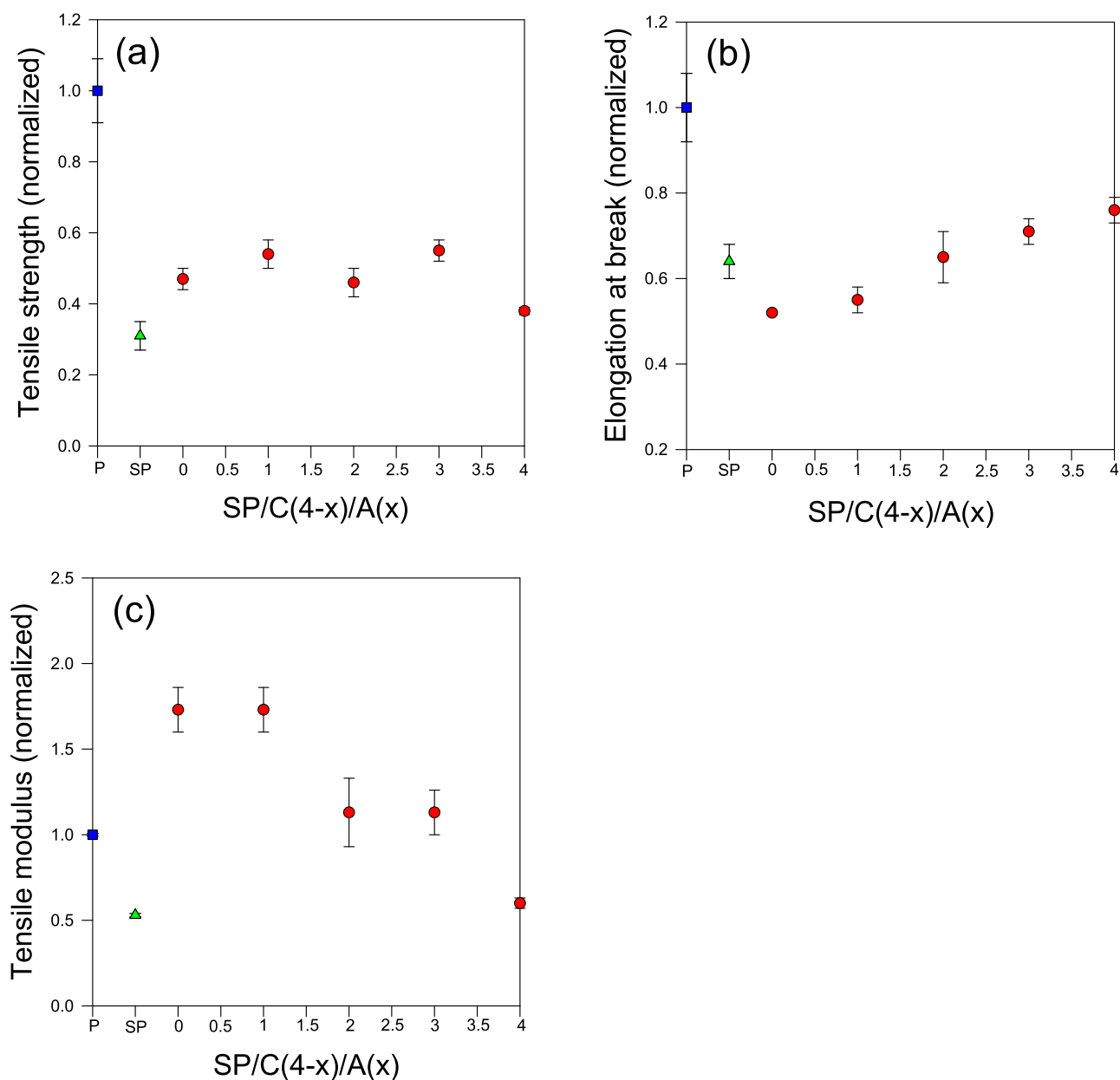
Figure 7. Mechanical properties (tensile mode) of PDMS/CNT/AgNW nanocomposites with different CNT/AgNW ratios (wt %/wt %): (a) tensile strength, (b) elongation at break, and (c) tensile modulus. P and SP denote PDMS and silicone oil-embedded PDMS, respectively.

The complex viscosities of the PDMS/CNT/AgNW nanocomposites with all ratios linearly decreased as a function of frequency. This indicates that the loss modulus/storage modulus ratio was constant regardless of the frequency, which is a common behavior of elastomeric materials.[62] The tan $\delta (G''/G')$ value represents the ratio of viscosity/elasticity. Low (<1) and high (>1) tan δ values indicate the elastic and viscous characteristics, respectively. The PDMS/CNT/AgNW nanocomposites with all compositions showed elastic behaviors in the whole frequency range, representing the solidlike characteristics with 3D network structures.

3.5. Electrical Properties of PDMS/CNT/AgNW Nanocomposites. The electrical properties of conductive nanofiller-incorporated polymer nanocomposites are attractive, which are influenced by factors such as filler dispersion, aspect ratio, concentration, and orientation. The effects of the nanofiller concentration ratios in the nanocomposites on the
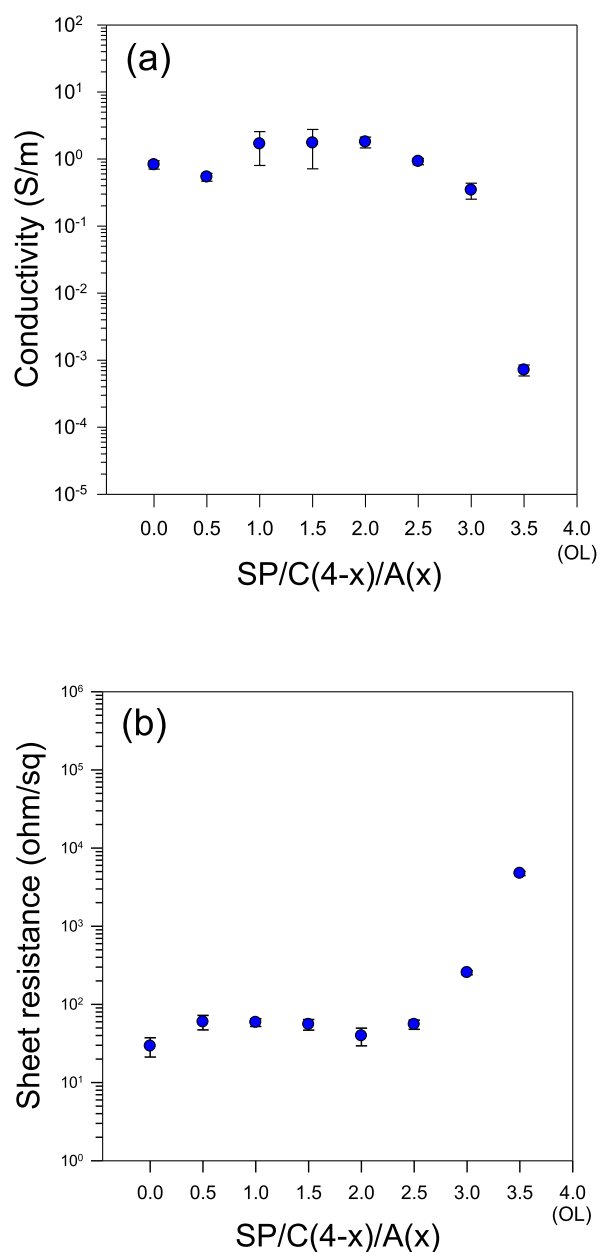
electrical conductivity and sheet resistance were examined, as shown in Figure 9. The electrical conductivity of the SP/C4/A0 nanocomposite was 0.82 S/m. As the AgNW concentration increased up to 2 wt % (SP/C2/A2), the electrical conductivity slightly increased up to 1.8 S/m. Beyond this concentration, the electrical conductivity of the nanocomposite decreased with the increasing AgNW content. The electrical conductivity of the SP/C0/A4 nanocomposite was not detected because of the absence of the conductive network of nanofillers. This result was in good agreement with the EDS mapping results. The CNT incorporation contributed to the good dispersion of AgNWs in the PDMS matrix during the IPA treatment, and the electrical path was generated along the CNT/AgNW network.[63] The formed electrical network complex of CNT/AgNW was more robust than that of singular fillers (CNTs and AgNWs). The reduction in electrical conductivity at 0.5 wt % AgNW (SP/C3.5/A0.5)
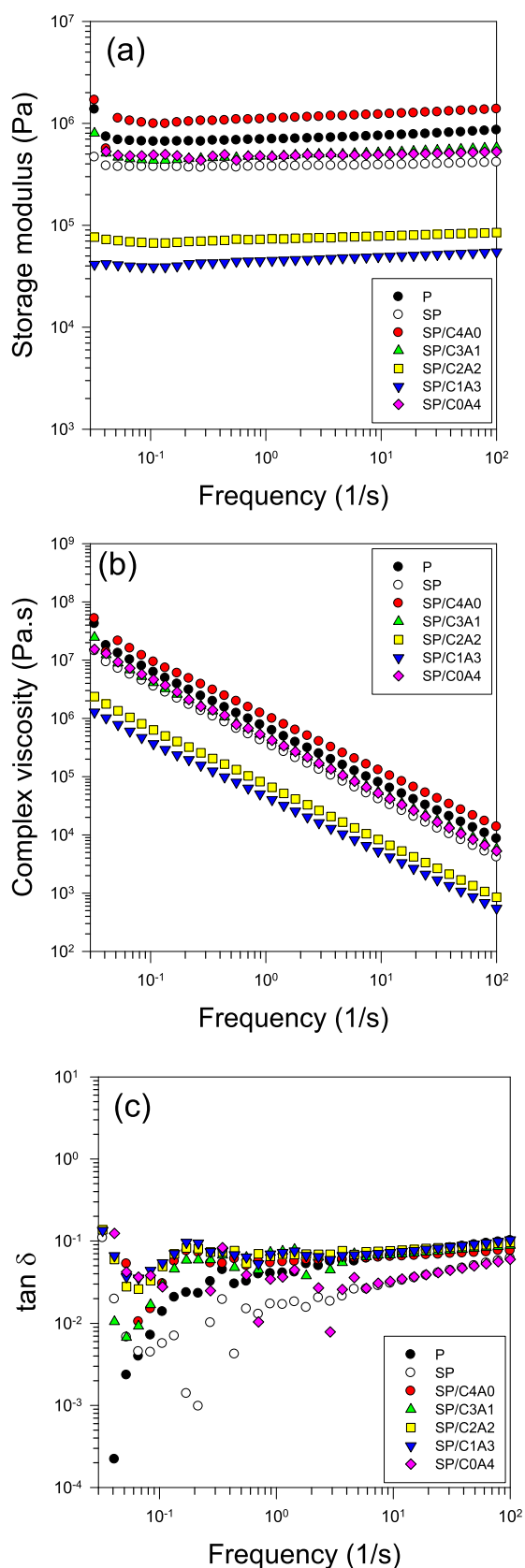
Figure 8. Storage modulus (a), complex viscosity (b), and tan δ(c) of PDMS with and without silicone oil and PDMS/CNT/AgNW nanocomposites with different CNT/AgNW ratios (wt %/wt %).

was caused by the inadequate ratio of CNTs/AgNWs. The small amount of AgNW (0.5 wt %) hindered the CNT/CNT

Figure 9. Electrical conductivity (a) and sheet resistance (b) of PDMS/CNT/AgNW nanocomposites with different CNT/AgNW concentrations (wt %/wt %). OL on the X-axis means "over limit."

network, while the synergy of the CNT/AgNW network was minimized. The electrical conductivity was minimized at low CNT concentrations because the AgNW/AgNW aggregates rarely interacted with CNTs. Because electrical resistance is inversely related to conductivity, the sheet resistance of the nanocomposite also showed the same trend as the electrical conductivity.

3.6. Cyclic Deformation Properties of PDMS/CNT/AgNW Nanocomposites. The cyclic deformation properties of the nanocomposites were measured at a tensile strain of 40% and frequency of 1 Hz for 5000 cycles, as shown in Figure 10 and Table 3. The mean stresses at the initial four cycles (σ_i), at the middle four cycles (σ_m), and at the final four cycles (σ_f) were determined from the data in Figures 10 and S6. The stresses for all the samples decreased as a function of the cycle. The initial stresses decreased and σ_f/σ_i increased with the
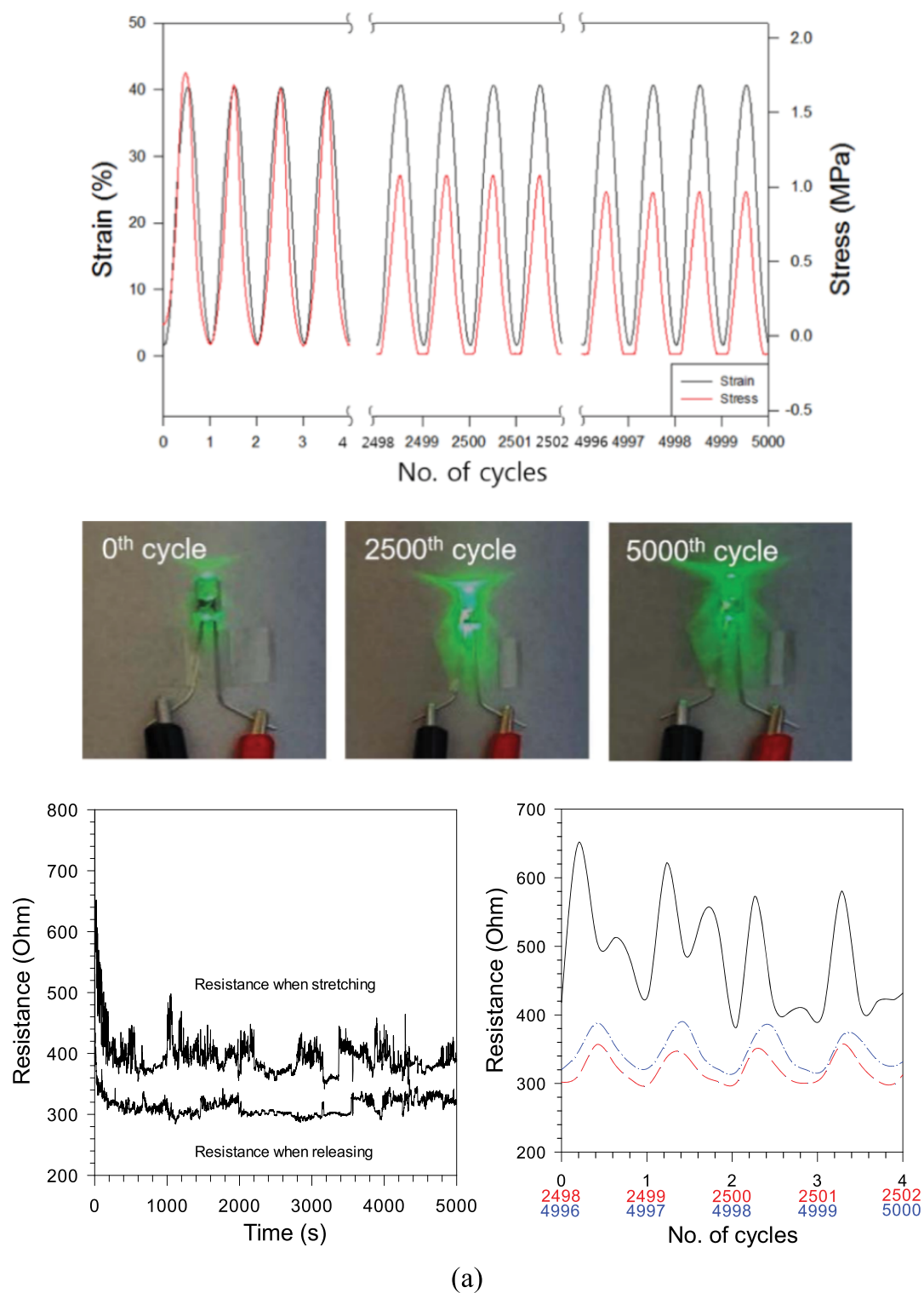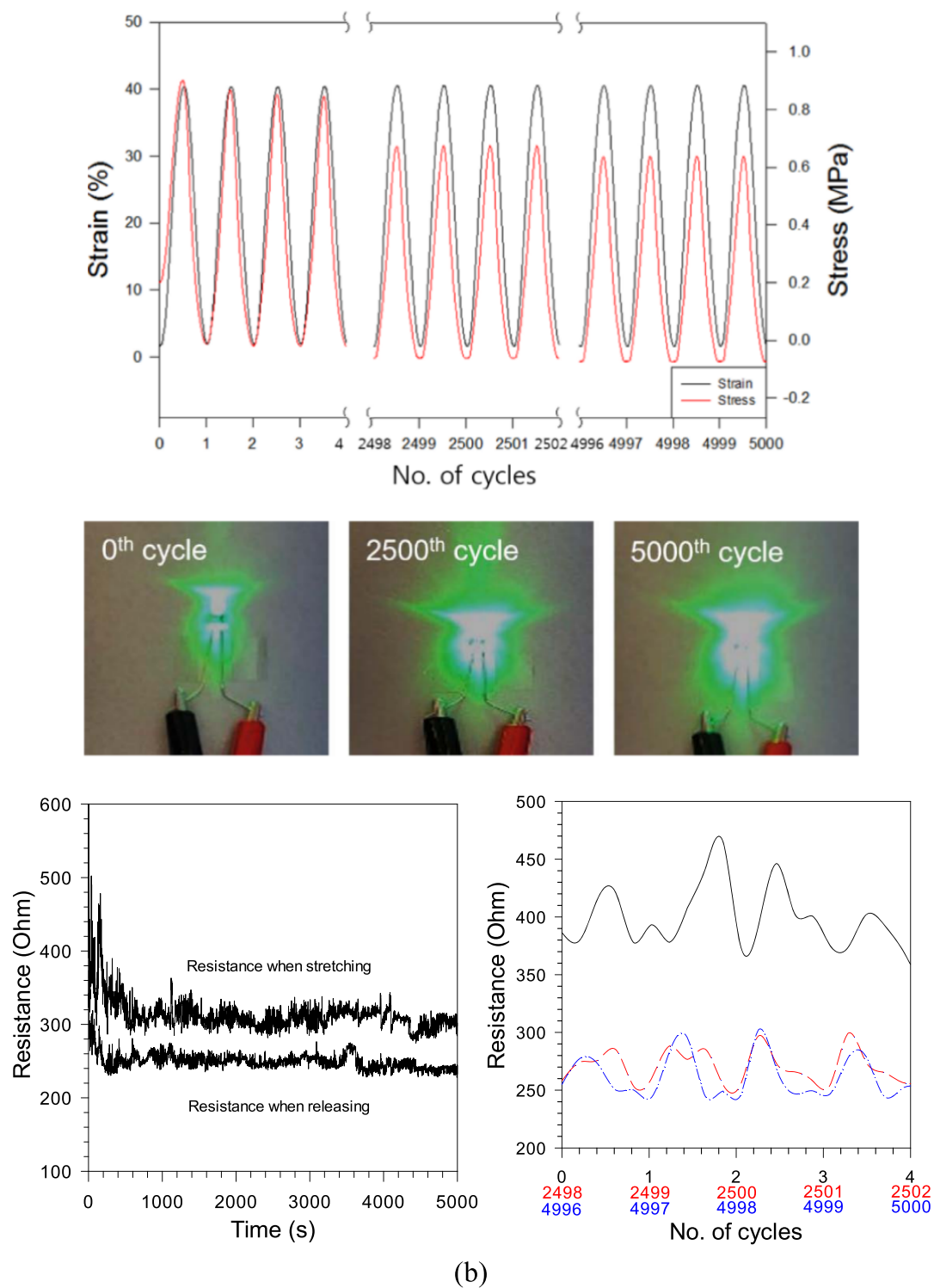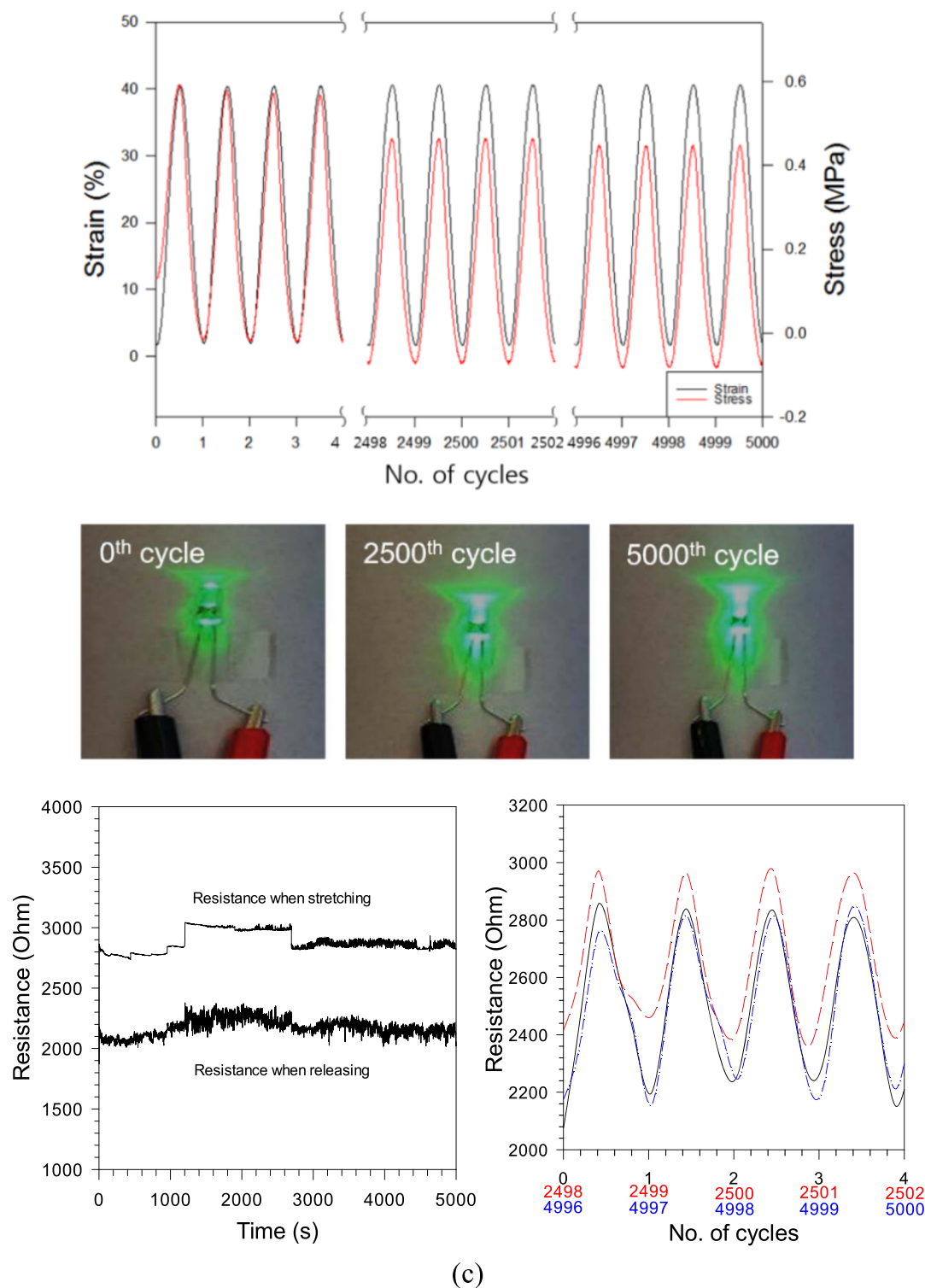
Figure 10. continued

Figure 10. continued

Figure 10. Dynamic properties of PDMS/CNT/AgNW nanocomposites with different CNT/AgNW ratios (wt %/wt %) during the cyclic strain test (stress change, LED light change, and resistance change). (a) SP/C3/A1, (b) SP/C2/A2, and (c) SP/C1/A3.

decreasing CNT concentration because the PDMS chains were released with increasing deformation cycles for the nanocomposites with low CNT content. Additionally, the interactions between CNT/CNT and CNT/PDMS decreased, thereby stretching the nanocomposites. The stress ratio σ_f/σ_i in the total number of cycles was divided into two sections to distinguish the stress ratio in the transient state (σ_m/σ_i) and the stress ratio in the steady state (σ_f/σ_m). The transient stress

ratio, defined here as the ratio of stresses in the first half of the total number of cycles, represents the unsteady state in which the stress changes instantaneously due to the abrupt imposition of strain. This shows the stress change due to the change in the arrangement of PDMS chains and nanofillers. On the other hand, the steady-state stress ratio shows the stress change due to the relaxation of the chain and the breakage of the nanofillers on fatigue, which is a practical stress ratio

Table 3. Stress Change of PDMS/CNT/AgNW Nanocomposites with Different CNT/AgNW Ratios (wt %/wt %) during the Cyclic Strain Test

|	stress at initial four cycles, σ_i	stress at middle four cycles, σ_m	Stress at final four cycles, σ_f	σ_m/σ_i	$\sigma f/\sigma m$	$\sigma f/\sigma i$
P	1.01	0.95	0.92	0.94	0.97	0.91
SP	1.02	0.98	0.96	0.96	0.98	0.94
SP/C4/A0	2.15	1.1	0.89	0.51	0.81	0.41
SP/C3/A1	1.65	1.08	0.97	0.65	0.9	0.59
SP/C2/A2	0.85	0.67	0.64	0.79	0.96	0.76
SP/C1/A3	0.57	0.46	0.45	0.81	0.98	0.79
SP/C0/A4	0.48	0.45	0.44	0.94	0.98	0.92

indicating whether it is suitable for long-term use properties. As the CNT content increases, the difference between the two ratios was substantial because well-dispersed CNTs in the matrix change into a preferred arrangement by repetitive deformation. Because the sinusoidal stress and strain curves are almost in-phase (phase angle δ: 3.6−5° during the final four cycles), as can be seen from the cyclic stress change in Figure 10, the tan δ values of all nanocomposites were close to zero (0.063−0.087). This indicates that the elasticity-dominant behavior of the nanocomposites was maintained after repeated deformation cycles. Not surprisingly, the tan δ values obtained from the dynamic tensile test showed similar results to those of the rheological shear test shown in Figure 8c.

The dynamic electrical conductivities of the PDMS/CNT/AgNW nanocomposites were measured synchronously during the cyclic strain tests. The electrical resistances of the PDMS/CNT/AgNW nanocomposites were monitored from 0 to 5000 cycles, and the light intensities of the LEDs were observed at 0, 2500, and 5000 cycles (Figures 10 and S7). The intensity of the light represents the electrical conductivity. The electrical resistances of all nanocomposites decreased, and the LED light intensity became stronger as a function of the repeated deformation cycle, representing the electrical stability. As shown in Figure 11, the nanofillers dispersed in the PDMS matrix slipped and broke during the cyclic strain tests. Afterward, the distance between the fillers became shorter,
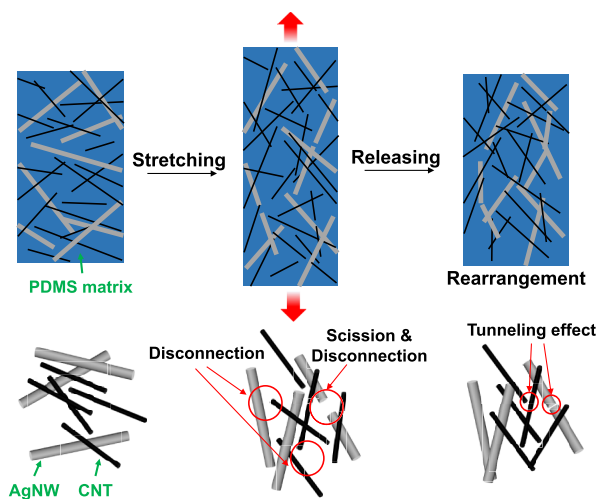
and the filler network was rearranged, thereby leading to the substantial filler network, which is called the tunneling effect.[64−66] The junctions between two conductive fibrous nanofillers are classified into three categories (complete contact, tunneling junction, and complete disconnection) based on their distance. The complete contact occurs where the distance (d) between two neighboring fillers is smaller than the diameter (D) of nanofillers. The tunneling effect is shown in the cases of $D < d <$ cutoff distance (C). Finally, the complete disconnection occurs at $d > C$. The d value depends on the type, composition, architecture, dimensions of nanofillers, and matrix type. In addition, the PDMS chains were released by the cyclic strain tests, and thus, the stress toward the nanofiller network was reduced at the identical strain of the final testing period. Thus, the electrical resistance decreased as a function of the deformation cycle, thereby bringing about electrical stability. The dynamic electrical conductivities of the nanocomposites were calculated based on eq 1 and using the mean electrical resistances when the resistances were stabilized after 2000 cycles, as shown in Figure 12. The trend for
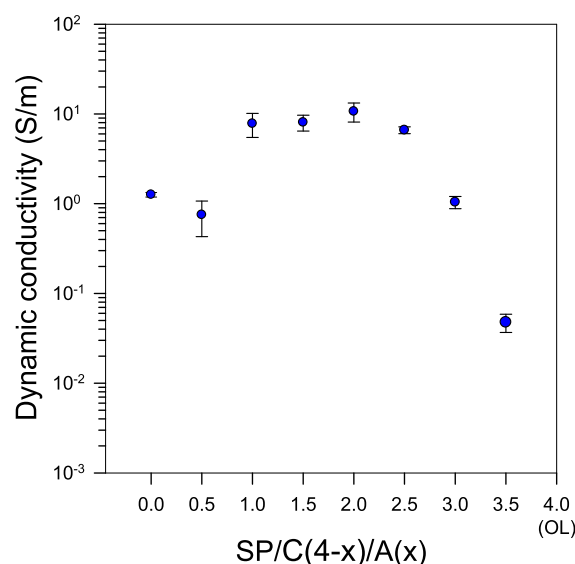
Figure 12. Dynamic electrical conductivity of PDMS/CNT/AgNW with different CNT/AgNW ratios (wt %/wt %) during the cyclic strain test.

dynamic electrical conductivities of the nanocomposites with different filler ratios was similar to that for the static electrical conductivities investigated in Figure 9. The highest dynamic electrical conductivity of the nanocomposite was 10 S/m for SP/C2/A2, which indicates the effect of the hybrid nanofillers.

4. CONCLUSIONS

In this study, the stretchable electrode nanocomposites with good electrical conductivities were fabricated by combining nanofillers, such as CNTs and AgNWs (synthesized by the polyol method), in the PDMS matrix. The combination of IPA, ultrasonication, and silicone oil enhanced the CNT dispersion and dispersion stability. The incorporation of CNTs into the silicone oil-coated PDMS/AgNW nanocomposites improved the AgNW dispersion in the PDMS matrix. The tensile modulus decreased, and the elongation at break increased with the decreasing CNT/AgNW ratio. Based on the rheological behaviors, the nanocomposites containing hybrid nanofillers

Figure 11. Network morphology of PDMS/CNT/AgNW nanocomposites during the cyclic strain test.

still exhibited elastic behavior owing to the stable filler network. The electrical conductivity of SP/C2/A2 was the highest (1.8 S/m). The tan δ values at the final four cycles were close to zero, indicating that the elastic behavior was still maintained after the cyclic strain tests (5000 cycles). The electrical conductivities of all nanocomposites increased during the cyclic strain tests because of the tunneling effect and strain-induced stress relaxation of the samples. The dynamic electrical conductivity of SP/C2/A2 stabilized after 2000 cycles was the highest (10 S/m) due to the effect of the hybrid fillers.

ASSOCIATED CONTENT

Supporting Information

The Supporting Information is available free of charge at https://pubs.acs.org/doi/10.1021/acsomega.1c04628.

Schematic diagram illustrating the purification process of AgNWs, dispersion stability of CNTs in different solvents such as water, EG, and IPA, dispersion of the PVP-capped AgNW in IPA, electrical properties of PDMS/CNT nanocomposites as a function of the CNT content, stress−strain curves of PDMS/CNT/AgNW nanocomposites with different CNT/AgNW ratios, dynamic properties of PDMS/CNT/AgNW with different CNT/AgNW ratios during cyclic strain tests, change of LED light according to cycles, tensile properties of PDMS/CNT nanocomposites as a function of the CNT content, and tensile properties of PDMS/CNT/AgNW nanocomposites (PDF)

AUTHOR INFORMATION

Corresponding Authors

Keon-Soo Jang − Department of Polymer Engineering, School of Chemical and Materials Engineering, The University of Suwon, Hwaseong, Gyeonggi 18323, Republic of Korea; orcid.org/0000-0002-0883-2683; Email: ksjang@suwon.ac.kr

Seong Jae Lee − Department of Polymer Engineering, School of Chemical and Materials Engineering, The University of Suwon, Hwaseong, Gyeonggi 18323, Republic of Korea; orcid.org/0000-0001-5514-3234; Email: sjlee@suwon.ac.kr

Authors

Tae Gon Kim − Department of Polymer Engineering, School of Chemical and Materials Engineering, The University of Suwon, Hwaseong, Gyeonggi 18323, Republic of Korea

Hyeon Sik Eom − Department of Polymer Engineering, School of Chemical and Materials Engineering, The University of Suwon, Hwaseong, Gyeonggi 18323, Republic of Korea

Jong Hwi Kim − Department of Polymer Engineering, School of Chemical and Materials Engineering, The University of Suwon, Hwaseong, Gyeonggi 18323, Republic of Korea; NanoChemTech Inc., Anseong, Gyeonggi 17502, Republic of Korea

Jik Kyo Jung − NanoChemTech Inc., Anseong, Gyeonggi 17502, Republic of Korea

Complete contact information is available at:
https://pubs.acs.org/10.1021/acsomega.1c04628

Notes

The authors declare no competing financial interest.

REFERENCES

(1) Omanović-Mikličanin, E.; Badnjević, A.; Kazlagić, A.; Hajlovac, M. Nanocomposites: A Brief Review. Health Technol. 2020, 10, 51−59.

(2) Kim, T. G.; Kim, J. M.; Jang, K.-S.; Lee, S. J. Dispersibility-Tailored Conductive Epoxy Nanocomposites with Silica Nanoparticle-Embedded Silver Nanowires. Polym. Test. 2021, 96, 107111.

(3) Bilotti, E.; Zhang, H.; Deng, H.; Zhang, R.; Fu, Q.; Peijs, T. Controlling the Dynamic Percolation of Carbon Nanotube Based Conductive Polymer Composites by Addition of Secondary Nanofillers: The Effect on Electrical Conductivity and Tuneable Sensing Behaviour. Compos. Sci. Technol. 2013, 74, 85−90.

(4) Park, O.-K.; Lee, S.-H.; Ku, B.-C.; Lee, J.-H. A Review of Graphene-based Polymer Nanocomposites. Polym. Sci. Technol. 2011, 22, 467−473.

(5) Lin, B.; Gelves, G. A.; Haber, J. A.; Sundararaj, U. Electrical, Rheological, and Mechanical Properties of Polystyrene/Copper Nanowire Nanocomposites. Ind. Eng. Chem. Res. 2007, 46, 2481−2487.

(6) Yoon, S.; Kim, H.-K. Cost-Effective Stretchable Ag Nanoparticles Electrodes Fabrication by Screen Printing for Wearable Strain Sensors. Surf. Coat. Technol. 2020, 384, 125308.

(7) Koo, J. H.; Kim, D. C.; Shim, H. J.; Kim, T.-H.; Kim, D.-H. Flexible and Stretchable Smart Display: Materials, Fabrication, Device Design, and System Integration. Adv. Funct. Mater. 2018, 28, 1801834.

(8) Kim, S. Y.; Noh, Y. J.; Yu, J. Improved Thermal Conductivity of Polymeric Composites Fabricated by Solvent-Free Processing for the Enhanced Dispersion of Nanofillers and a Theoretical Approach for Composites Containing Multiple Heterogeneities and Geometrized Nanofillers. Compos. Sci. Technol. 2014, 101, 79−85.

(9) Zhang, Q.; Fang, F.; Zhao, X.; Li, Y.; Zhu, M.; Chen, D. Use of Dynamic Rheological Behavior to Estimate the Dispersion of Carbon Nanotubes in Carbon Nanotube/Polymer Composites. J. Phys. Chem. B 2008, 112, 12606−12611.

(10) Tang, L.-C.; Wan, Y.-J.; Yan, D.; Pei, Y.-B.; Zhao, L.; Li, Y.-B.; Wu, L.-B.; Jiang, J.-X.; Lai, G.-Q. The Effect of Graphene Dispersion on the Mechanical Properties of Graphene/Epoxy Composites. Carbon 2013, 60, 16−27.

(11) Šupová, M.; Martynková, G. S.; Barabaszová, K. Effect of Nanofillers Dispersion in Polymer Matrices: A Review. Sci. Adv. Mater. 2011, 3, 1−25.

(12) Pandey, A. K.; Pal, T.; Sharma, R.; Kar, K. K. Study of Matrix−Filler Interaction through Correlations between Structural and Viscoelastic Properties of Carbonous-Filler/Polymer-Matrix Composites. J. Appl. Polym. Sci. 2020, 137, 48660.

(13) Harris, P. J. F. Carbon Nanotube Composites. Int. Mater. Rev. 2004, 49, 31−43.

(14) Cwirzen, A.; Habermehl-Cwirzen, K.; Penttala, V. Surface Decoration of Carbon Nanotubes and Mechanical Properties of Cement/Carbon Nanotube Composites. Adv. Cem. Res. 2008, 20, 65−73.

(15) Krause, B.; Barbier, C.; Kunz, K.; Pötschke, P. Comparative Study of Singlewalled, Multiwalled, and Branched Carbon Nanotubes Melt Mixed in Different Thermoplastic Matrices. Polymer 2018, 159, 75−85.

(16) Zhou, Y.; Zhou, X.; Ge, C.; Zhou, W.; Zhu, Y.; Xu, B. Branched Carbon Nanotube/Carbon Nanofiber Composite for Supercapacitor Electrodes. Mater. Lett. 2019, 246, 174−177.

(17) Zhang, Q.; Huang, J.-Q.; Qian, W.-Z.; Zhang, Y.-Y.; Wei, F. The Road for Nanomaterials Industry: A Review of Carbon Nanotube

Production, Post-Treatment, and Bulk Applications for Composites and Energy Storage. *Small* **2013**, *9*, 1237−1265.

(18) Ke, K.; Sang, Z.; Manas-Zloczower, I. Stretchable Elastomer Composites with Segregated Filler Networks: Effect of Carbon Nanofiller Dimensionality. *Nanoscale Adv.* **2019**, *1*, 2337−2347.

(19) Ke, K.; Solouki Bonab, V.; Yuan, D.; Manas-Zloczower, I. Piezoresistive Thermoplastic Polyurethane Nanocomposites with Carbon Nanostructures. *Carbon* **2018**, *139*, 52−58.

(20) Arif, M. F.; Kumar, S.; Gupta, T. K.; Varadarajan, K. M. Strong Linear-Piezoresistive-Response of Carbon Nanostructures Reinforced Hyperelastic Polymer Nanocomposites. *Compos. Appl. Sci. Manuf.* **2018**, *113*, 141−149.

(21) Bai, L.; Bai, Y.; Zheng, J. Improving the Filler Dispersion and Performance of Silicone Rubber/Multi-Walled Carbon Nanotube Composites by Noncovalent Functionalization of Polymethylphenyl-siloxane. *J. Mater. Sci.* **2017**, *52*, 7516−7529.

(22) Ma, P.-C.; Siddiqui, N. A.; Marom, G.; Kim, J.-K. Dispersion and Functionalization of Carbon Nanotubes for Polymer-Based Nanocomposites: A Review. *Compos. Appl. Sci. Manuf.* **2010**, *41*, 1345−1367.

(23) Jiménez-Suárez, A.; Campo, M.; Gaztelumendi, I.; Markaide, N.; Sánchez, M.; Ureña, A. The Influence of Mechanical Dispersion of MWCNT in Epoxy Matrix by Calendering Method: Batch Method versus Time Controlled. *Compos. B Eng.* **2013**, *48*, 88−94.

(24) Jung, W. R.; Choi, J. H.; Lee, N.; Shin, K.; Moon, J.-H.; Seo, Y.-S. Reduced Damage to Carbon Nanotubes during Ultrasound-Assisted Dispersion as a Result of Supercritical-Fluid Treatment. *Carbon* **2012**, *50*, 633−636.

(25) Chen, H.; Jacobs, O.; Wu, W.; Rüdiger, G.; Schädel, B. Effect of Dispersion Method on Tribological Properties of Carbon Nanotube Reinforced Epoxy Resin Composites. *Polym. Test.* **2007**, *26*, 351−360.

(26) Liu, Z. Y.; Xu, S. J.; Xiao, B. L.; Xue, P.; Wang, W. G.; Ma, Z. Y. Effect of Ball-Milling Time on Mechanical Properties of Carbon Nanotubes Reinforced Aluminum Matrix Composites. *Compos. Appl. Sci. Manuf.* **2012**, *43*, 2161−2168.

(27) Yellampalli, S. *Carbon Nanotubes: Synthesis, Characterization, Applications*; BoD—Books on Demand, 2011.

(28) Khan, M. U.; Gomes, V. G.; Altarawneh, I. S. Synthesizing Polystyrene/Carbon Nanotube Composites by Emulsion Polymer-ization with Non-Covalent and Covalent Functionalization. *Carbon* **2010**, *48*, 2925−2933.

(29) Gong, X.; Liu, J.; Baskaran, S.; Voise, R. D.; Young, J. S. Surfactant-Assisted Processing of Carbon Nanotube/Polymer Composites. *Chem. Mater.* **2000**, *12*, 1049−1052.

(30) Vaisman, L.; Wagner, H. D.; Marom, G. The Role of Surfactants in Dispersion of Carbon Nanotubes. *Adv. Colloid Interface Sci.* **2006**, *128−130*, 37−46.

(31) Le, V. T.; Ngo, C. L.; Le, Q. T.; Ngo, T. T.; Nguyen, D. N.; Vu, M. T. Surface Modification and Functionalization of Carbon Nanotube with Some Organic Compounds. *Adv. Nat. Sci. Nanosci. Nanotechnol.* **2013**, *4*, 035017.

(32) Beheshtian, J.; Peyghan, A. A.; Bagheri, Z. Carbon Nanotube Functionalization with Carboxylic Derivatives: A DFT Study. *J. Mol. Model.* **2013**, *19*, 391−396.

(33) Kim, J. M.; Jang, K. S.; Lee, S. J. Electrically Conductive Polystyrene Nanocomposites Incorporated with Aspect Ratio-Controlled Silver Nanowires. *J. Appl. Polym. Sci.* **2019**, *136*, 47927.

(34) Lau, K. S.; Chin, S. X.; Tan, S. T.; Lim, F. S.; Chang, W. S.; Yap, C. C.; Jumali, M. H. H.; Zakaria, S.; Chook, S. W.; Chia, C. H. Silver Nanowires as Flexible Transparent Electrode: Role of PVP Chain Length. *J. Alloys Compd.* **2019**, *803*, 165−171.

(35) Lin, J.-Y.; Hsueh, Y.-L.; Huang, J.-J. The Concentration Effect of Capping Agent for Synthesis of Silver Nanowire by Using the Polyol Method. *J. Solid State Chem.* **2014**, *214*, 2−6.

(36) Zhang, P.; Wyman, I.; Hu, J.; Lin, S.; Zhong, Z.; Tu, Y.; Huang, Z.; Wei, Y. Silver Nanowires: Synthesis Technologies, Growth Mechanism and Multifunctional Applications. *Mater. Sci. Eng., B* **2017**, *223*, 1−23.

(37) Coskun, S.; Aksoy, B.; Unalan, H. E. Polyol Synthesis of Silver Nanowires: An Extensive Parametric Study. *Cryst. Growth Des.* **2011**, *11*, 4963−4969.

(38) Qi, D.; Zhang, K.; Tian, G.; Jiang, B.; Huang, Y. Stretchable Electronics Based on PDMS Substrates. *Adv. Mater.* **2021**, *33*, 2003155.

(39) Peng, S.; Yu, Y.; Wu, S.; Wang, C.-H. Conductive Polymer Nanocomposites for Stretchable Electronics: Material Selection, Design, and Applications. *ACS Appl. Mater. Interfaces* **2021**, *13*, 43831−43854.

(40) Hassouneh, S. S.; Yu, L.; Skov, A. L.; Daugaard, A. E. Soft and Flexible Conductive PDMS/MWCNT Composites. *J. Appl. Polym. Sci.* **2017**, *134* (). https://doi.org/ DOI: 10.1002/app.44767.

(41) Lee, P.; Lee, J.; Lee, H.; Yeo, J.; Hong, S.; Nam, K. H.; Lee, D.; Lee, S. S.; Ko, S. H. Highly Stretchable and Highly Conductive Metal Electrode by Very Long Metal Nanowire Percolation Network. *Adv. Mater.* **2012**, *24*, 3326−3332.

(42) Fan, Y. J.; Meng, X. S.; Li, H. Y.; Kuang, S. Y.; Zhang, L.; Wu, Y.; Wang, Z. L.; Zhu, G. Stretchable Porous Carbon Nanotube-Elastomer Hybrid Nanocomposite for Harvesting Mechanical Energy. *Adv. Mater.* **2017**, *29*, 1603115.

(43) Zhang, F.; Wu, S.; Peng, S.; Sha, Z.; Wang, C. H. Synergism of Binary Carbon Nanofibres and Graphene Nanoplates in Improving Sensitivity and Stability of Stretchable Strain Sensors. *Compos. Sci. Technol.* **2019**, *172*, 7−16.

(44) Shin, H.; Sharma, B. K.; Lee, S. W.; Lee, J.-B.; Choi, M.; Hu, L.; Park, C.; Choi, J. H.; Kim, T. W.; Ahn, J.-H. Stretchable Electroluminescent Display Enabled by Graphene-Based Hybrid Electrode. *ACS Appl. Mater. Interfaces* **2019**, *11*, 14222−14228.

(45) Chen, S.; Wei, Y.; Wei, S.; Lin, Y.; Liu, L. Ultrasensitive Cracking-Assisted Strain Sensors Based on Silver Nanowires/ Graphene Hybrid Particles. *ACS Appl. Mater. Interfaces* **2016**, *8*, 25563−25570.

(46) Liu, S.; Lin, Y.; Wei, Y.; Chen, S.; Zhu, J.; Liu, L. A High Performance Self-Healing Strain Sensor with Synergetic Networks of Poly(ε-Caprolactone) Microspheres, Graphene and Silver Nanowires. *Compos. Sci. Technol.* **2017**, *146*, 110−118.

(47) Dong, X.; Wei, Y.; Chen, S.; Lin, Y.; Liu, L.; Li, J. A Linear and Large-Range Pressure Sensor Based on a Graphene/Silver Nanowires Nanobiocomposites Network and a Hierarchical Structural Sponge. *Compos. Sci. Technol.* **2018**, *155*, 108−116.

(48) Li, Y.; Wang, S.; Xiao, Z.-c.; Yang, Y.; Deng, B.-w.; Yin, B.; Ke, K.; Yang, M.-b. Flexible TPU Strain Sensors with Tunable Sensitivity and Stretchability by Coupling AgNWs with RGO. *J. Mater. Chem. C* **2020**, *8*, 4040−4048.

(49) Zhu, L.; Wang, Y.; Mei, D.; Ding, W.; Jiang, C.; Lu, Y. Fully Elastomeric Fingerprint-Shaped Electronic Skin Based on Tunable Patterned Graphene/Silver Nanocomposites. *ACS Appl. Mater. Interfaces* **2020**, *12*, 31725−31737.

(50) Wei, Y.; Chen, S.; Dong, X.; Lin, Y.; Liu, L. Flexible Piezoresistive Sensors Based on "Dynamic Bridging Effect" of Silver Nanowires toward Graphene. *Carbon* **2017**, *113*, 395−403.

(51) Ke, K.; Yue, L.; Shao, H.; Yang, M.-B.; Yang, W.; Manas-Zloczower, I. Boosting Electrical and Piezoresistive Properties of Polymer Nanocomposites via Hybrid Carbon Fillers: A Review. *Carbon* **2021**, *173*, 1020−1040.

(52) Lisensky, G. C.; Campbell, D. J.; Beckman, K. J.; Calderon, C. E.; Doolan, P. W.; Ottosen, R. M.; Ellis, A. B. Replication and Compression of Surface Structures with Polydimethylsiloxane Elastomer. *J. Chem. Educ.* **1999**, *76*, 537.

(53) Lee, S.-B.; Jeong, B.-H.; Yi, J.-W.; Lee, W.-O.; Um, M.-K. Quantitative Dispersion Evaluation of Carbon Nanotubes Reinforced Polymer Nano-composites. *Polymer* **2011**, *35*, 60−65.

(54) Kim, J.-H.; Ma, H.-Y.; Yang, S.-Y.; Kim, S.-J. Analysis of Electrical and Physical Property of the PU/MWNT Film and Dispersion Characteristics of MWNT According to the Solvent. *Text. Color. Finish.* **2012**, *24*, 69−78.

(55) Kim, J. H.; Hwang, J.-Y.; Hwang, H. R.; Kim, H. S.; Lee, J. H.; Seo, J.-W.; Shin, U. S.; Lee, S.-H. Simple and Cost-Effective Method

of Highly Conductive and Elastic Carbon Nanotube/Polydimethylsi-loxane Composite for Wearable Electronics. *Sci. Rep.* **2018**, *8*, 1375.

(56) Wang, J.; Yan, C.; Kang, W.; Lee, P. S. High-Efficiency Transfer of Percolating Nanowire Films for Stretchable and Transparent Photodetectors. *Nanoscale* **2014**, *6*, 10734−10739.

(57) Korayem, A. H.; Barati, M. R.; Simon, G. P.; Zhao, X. L.; Duan, W. H. Reinforcing Brittle and Ductile Epoxy Matrices Using Carbon Nanotubes Masterbatch. *Compos. Appl. Sci. Manuf.* **2014**, *61*, 126−133.

(58) Jen, Y.-M.; Wang, Y.-C. Stress Concentration Effect on the Fatigue Properties of Carbon Nanotube/Epoxy Composites. *Compos. B Eng.* **2012**, *43*, 1687−1694.

(59) Ludeelerd, P.; Niamlang, S.; Kunaruksapong, R.; Sirivat, A. Effect of Elastomer Matrix Type on Electromechanical Response of Conductive Polypyrrole/Elastomer Blends. *J. Phys. Chem. Solids* **2010**, *71*, 1243−1250.

(60) Hong, J.; Park, D. W.; Shim, S. E. Electrical, Thermal, and Rheological Properties of Carbon Black and Carbon Nanotube Dual Filler-Incorporated Poly(Dimethylsiloxane) Nanocomposites. *Macromol. Res.* **2012**, *20*, 465−472.

(61) Shim, S. E.; Isayev, A. I. Rheology and Structure of Precipitated Silica and Poly(Dimethyl Siloxane) System. *Rheol. Acta* **2004**, *43*, 127−136.

(62) Jung, H. S.; Kwon, S. H.; Choi, H. J.; Jung, J. H.; Kim, Y. G. Magnetic Carbonyl Iron/Natural Rubber Composite Elastomer and Its Magnetorheology. *Compos. Struct.* **2016**, *136*, 106−112.

(63) Jing, M.-x.; Han, C.; Li, M.; Shen, X.-q. High Performance of Carbon Nanotubes/Silver Nanowires-PET Hybrid Flexible Transparent Conductive Films via Facile Pressing-Transfer Technique. *Nanoscale Res. Lett.* **2014**, *9*, 588.

(64) Hu, N.; Karube, Y.; Yan, C.; Masuda, Z.; Fukunaga, H. Tunneling Effect in a Polymer/Carbon Nanotube Nanocomposite Strain Sensor. *Acta Mater.* **2008**, *56*, 2929−2936.

(65) Luo, S.; Liu, T. Structure−Property−Processing Relationships of Single-Wall Carbon Nanotube Thin Film Piezoresistive Sensors. *Carbon* **2013**, *59*, 315−324.

(66) Amjadi, M.; Pichitpajongkit, A.; Lee, S.; Ryu, S.; Park, I. Highly Stretchable and Sensitive Strain Sensor Based on Silver Nanowire−Elastomer Nanocomposite. *ACS Nano* **2014**, *8*, 5154−5163.